Progress In Electromagnetics Research, PIER 16, 117–151, 1997

A DEDICATED RADAR IMAGING STATISTICAL MODEL OF THE SINCLAIR MATRIX INITIALLY CHARACTERISED IN AN ANECHOÏC CHAMBER: APPLICATION TO THE HUYNEN PARAMETERS SENSITIVITY ANALYSIS

L. Priou, B. Uguen, and G. Chassay

L.C.S.T.-U.R.A. 834-I.N.S.A.
20, avenue des buttes de Coësmes
35043 Rennes Cedex, France

INTRODUCTION

Nowadays, thanks to radar polarimetry and especially target decomposition theorems, it is possible to extract physical information from observed data and consequently to classify crops or identify a fluctuating target. Among the target decomposition theorems, we distinguish

two classes. The first class gathers the theorems which are based on the decomposition of the Mueller matrix (Huynen Decomposition [DISS]) or of the coherency matrix [1] whereas the second class gathers coherent decomposition of the Sinclair matrix [1].

Other applications of radar polarimetry concerns the identification and classification of scattering phenomenon which are induced by an incident wave on a fixed target (reflection, double interaction, ...) [2]. Indeed, since the advent of the vectorial measurement systems, it has been possible to measure the whole Sinclair matrix in the frequency domain and consequently to construct any polarimetric parameter holographic radar images of targets characterised in an Anechoïc Chamber (AC). However, when characterising a target in an AC, its scattering matrix is systematically erroneous by a random signal which is generated by the internal noise sources of the measurement channel. Such an error can lead for specific targets to a deep degradation in the performance of a classification tool using HPs whatever the target backscattered power is.

In this paper, we develop a statistical model of the Noise Sinclair Matrix (NSM) in the holographic radar images domain to characterize the sensitivity of the HPs versus the internal noise sources of the measurement channel. On these grounds, Section I presents a brief review of the Huynen phenomenological theory. Then Section II proposes first in the frequency domain then in the spatial domains, a statistical and polarimetric model of the measurement channel noise sources. At last, Section III underlines, by both simulation and experimental results, the great HPs sensitivity for specific targets and proposes, in the frequential and spatial domains, a prediction model of any HP sensitivity, based on the analysis of its simulated distribution function.

1. THEORETICAL REVIEW

1.1 The Desying and the Euler Parameters

The Sinclair matrix $[S]$ syntheses both the polarimetric and the electromagnetic properties of a target. This matrix defines four coefficients, each coefficient corresponding to a given polarisation channel of a given polarimetric basis HV:

$$[S]_{HV} = \begin{bmatrix} S_{hh} & S_{hv} \\ S_{vh} & S_{vv} \end{bmatrix} \tag{1}$$

However, this representation is target orientation angle dependent. An identical target with the same exposure but with a different orientation angle would give a different signature. To eliminate this observation bias, that is to say to get a single Sinclair matrix whatever the target orientation angle facing the basis orientation angle is, we have to desy the target. Mathematically, it consists in resolving the Kennaugh's equation [3].

$$[S]_{hv}\,\hat{x} = \hat{x}^* \tag{2}$$

Its resolution leads to a definition of a new polarimetric basis in which the Sinclair matrix is diagonalised:

$$[S]_d = [E(\tau_m)]^T \underbrace{[R(\varphi_m)]^T \begin{bmatrix} S_{hh} & S_{hv} \\ S_{vh} & S_{vv} \end{bmatrix} [R(\varphi_m)]}_{\substack{\text{Target orientation angle} \\ \text{independent matrix}}} [E(\tau_m)] \tag{3}$$

that is to say

$$[S]_d = e^{j\rho} \begin{bmatrix} me^{2jv} & 0 \\ 0 & m\tan^2\gamma e^{-2jv} \end{bmatrix} \tag{4}$$

φ_m is the orientation angle. It represents the angle of the rotation which has to be applied to the polarimetric basis to eliminate the tilt bias. The $[E]$ matrix is the ellipticity matrix which is defined by a single angle τ_m. This angle is relevant of the target symmetry/non-symmetry property. From the non-zero coefficients of the diagonalised matrix $[S]_d$, 3 others parameters are derived, the skip angle υ, the polarisability angle γ and the magnitude m. They define with φ_m and τ_m the Euler parameters.

1.2 Huynen Phenomenological Theory

The objective of the Huynen phenomenological theory is to extract from the target polarimetric analysis, its intrinsic characteristics. On those grounds, Huynen defines from the parameters τ_m, m, γ, and υ, 9 parameters linked together by 4 independent relations. These parameters are target orientation angle independent. As a consequence, whatever the orientation of the target facing the line of sight is, they will give the same information.

The 4 independent relations define 3 generators called the symmetric generator $(2A_0)$, the non-symmetric generator $(B_0 - B)$ and the irregularity generator $(B_0 + B)$. The cancelling of these generators leads to a cancelling of the whole set of HPs.

Moreover, according to this theory, any target is composed of a symmetric part and a non-symmetric part. Each part is described by a HPs set. To both the symmetric part and the non-symmetric part corresponds 3 parameters including a generator. The two others parameters are responsible for the analysis of the part they are attached to [4].

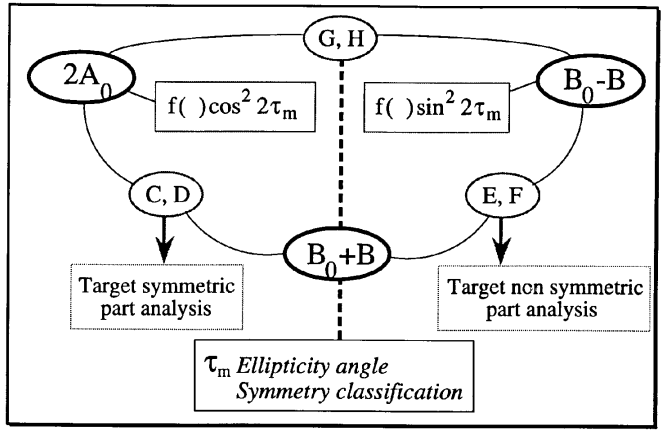

Figure 1. Structural diagram of a target.

A non zero value of any C, D, E or F parameter leads to a non-zero irregularity generator. One is usual to say that this target presents some irregularity.

The two last HPs parameters (G and H), are considered by Huynen as some coupling parameters between the symmetric and the non-symmetric parts.

The following table sums up the physical meaning of each HP.

$2A_0$ is the generator target symmetry	:	$2A_0 = 2Q_0 f \cos^2 2\tau_m$
$B_0 - B$ is the generator of target non-symmetry	:	$B_0 - B = 2Q_0 f sin^2 2\tau_m$
$B_0 + B$ is the generator of target irregularity	:	$B_0 + B = 2Q_0(\cos^2 2\gamma + \sin^2 2\gamma \sin^2 2\upsilon)$
C is the shape factor. It is maximum for a wire	:	$C = 2Q_0 \cos 2\gamma \cos 2\tau_m$
D is a measure of local curvature difference [1]	:	$D = Q_0 \sin^2 2\gamma \sin 4\upsilon \cos 2\tau_m$
E is a measure of the surface torsion	:	$E = -Q_0 \sin^2 2\gamma \sin 4\upsilon \sin 2\tau_m$
F is a measure target helicity	:	$F = 2Q_0 \cos 2\gamma \sin 2\tau_m$
G and H are coupling parameters	:	$G = Q_0 f \sin 4\tau_m$ and $H = 0$

where

$$Q_0 = \frac{m^2}{4\cos^4\gamma} \qquad f = 1 - \sin^2 2\gamma \sin^2 2\upsilon$$

2. A STATISTICAL MODEL OF THE NSM

2.1 In the Frequency Domain

The objective of this first section is to define, in the frequency domain, the statistical properties of the NSM which is added to the exact target Sinclair matrix. The so-defined random signal is called the noise Sinclair matrix (NSM).

We distinguish three parts in this section. The first part presents the theoretical characteristics of the NSM and the second part, the experimental results which corroborate the whole model in the frequency domain. We conclude this section by a performance evaluation of this statistical model.

[1] This assertion was corroborated by the work of Chaudhuri and Boerner [5].

2.1.1 Theoretical Characteristics of the NSM Statistical Model

Let's consider three Sinclair matrices:

—the $[S(f)]$ measured target Sinclair matrix
—the $[S_0(f)]$ theoretical target Sinclair matrix
—the $[N(f)]$ noise Sinclair matrix

The $[S(f)]$ Sinclair matrix is calibrated with the Wiesbeck calibration method [6], Note that the empty AC Sinclair matrix is previously subtracted from the measured target Sinclair matrix.

The $[S_0(f)]$ Sinclair matrix is equal to the theoretical target Sinclair matrix. This assertion implies a perfect polarimetric calibration which allows our study to focus on the NSM statistical properties. As a consequence, we don't consider in this work the systematic errors consequences on the Huynen parameters values. Only the statistical errors consequences are studied.

The $[N(f)]$ Sinclair matrix quantifies the internal noise sources effect on the cross- and co-polarised channels of the measurement basis. The internal noise sources are assumed to be of additive nature.

The developed statistical model stipulates that the calibrated Sinclair matrix of a **fixed** target is the sum of the theoretical target Sinclair matrix and of the NSM:

$$[S(f)] = [S_0(f)] + [N(f)] \tag{5}$$

Each NSM coefficient $N_{pq}(f)$ is a random, ergodic and stationary process with a zero average and a gaussian distribution. Each random process depends on two variables: the space variable, common with the deterministic signals (frequency f), and a second one denoting the random nature of the process (variable ζ). Afterwards, we'll mean by $N_{pq}(f)$ the random process $N_{pq}(f, \zeta)$ and by $N_{pq}(f_0)$ the random variable $N_{pq}(f_0, \zeta)$.

2.1.2 Validation of the NSM Statistical Model

$\diamond$ The $N_{pq}(f)$ statistical distribution

Illustrating the histogram of the random variable samples is not sufficient to determine with precision its statistical distribution nature. We prefer work on its P-plot representation. This kind of representation illustrates a theoretical random variable Y as a function of a random variable X, defined by the studied signal samples. If a straight

line is visualised, the X statistical distribution and the Y statistical distribution are identical.

To construct P-plots representations, one has to provide a sufficient number of samples of the studied signal. The measured samples represent a large spread of the possible random variable realisations, from which we deduce the statistical distribution of the studied random variable. Owing to the length of the acquisition time of a single Sinclair matrix, we limit the measured Sinclair matrices number to 1500. To get rid of the AC background, we define a gating which is centred round the target support. The frequency domain is the X band ($[8 \ldots 12]$ GHz) whereas the frequency step is set to 20 MHz and the f_0 work frequency to 10 GHz. The Sinclair matrix of the empty AC is previously subtracted from the whole measured Sinclair matrix. The measured Sinclair matrix is calibrated with the Wiesbeck calibration method. Note that this mathematical operation preserves, as the gating, the distribution nature of the studied random processes owing to the linear feature of these transforms [7].

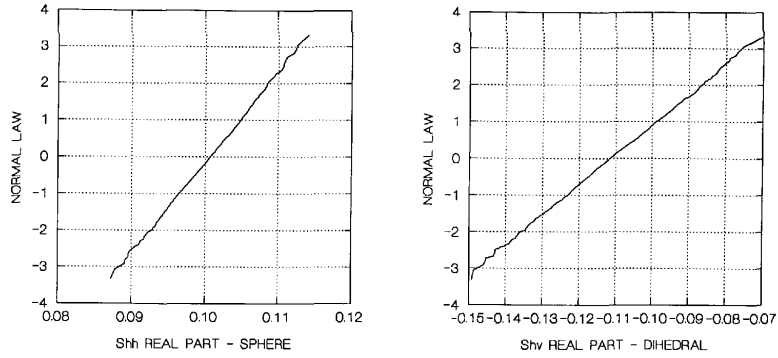

Figure 2. Statistical distributions.

The preceding figures illustrates the real part statistical distribution of both the S_{hh} coefficient of a 5 cm radius sphere and the S_{hv} coefficient of a 45 degrees tilted diplane whose dimensions are 9 and 10 cm long.

Whatever the studied target is, each of these figures illustrates a straight line for a Y gaussian random variable and consequently underlines that the studied statistical distributions are gaussian. One must notice that the observed oscillations at both straight line extremities

result from the poor probability of the studied signal samples to take such values. The Kolmogorov-Smirnov test was also applied to test the S_{hh}-sphere distribution. It identifies a gaussian distribution with a probability of 0.80, whereas the error is less than 5%. By assuming that the four $N_{pq}(f)$ random processes are ergodic, we conclude that these random processes are gaussian.

◇ Demonstration of the additive feature of the internal noise sources

This demonstration is performed at a l0 GHz frequency. The $N_{pq}(f)$ process quantifies the internal noise sources effect on the measurement basis channel defined by the pq polarization couple.

- $N_{pq}(f)$ processes averages

	HH	HV	VH	VV
REAL part (dBm^2)	-46.1	-47.2	-48.2	-46.2
IMAG part (dBm^2)	-46.2	-48.3	-47.1	-46.3

Table 1. Averages of the four $N_{pq}(f_0)$ random variables.

One can observe that none of these averages rises above $-46\ \mathrm{dBm}^2$. Taking into account the low values of these averages, we admit afterwards that the corresponding random variables are approximately centred. This conclusion may be extended to the whole frequency domain owing to the stationary feature of the analysed processes. As a consequence, the mean of the measured Sinclair matrices $[\,S_0(f)\,]$ only depends on the studied target.

- $N_{pq}(f)$ processes Standard Deviation (StD)

For each polarisation channel, the following table presents the corresponding StD. Four targets are studied: the sphere and the 45 degrees tilted dihedral which have been previously described, an horizontal wire and the nose of a missile whose description is given by Figure 6. We compare the obtained results to the StD of each $N_{pq}(f)$ random variable.

TARGETS	STANDARD DEVIATIONS (x10^{-3})							
	S_{hh}		S_{hv}		S_{vh}		S_{vv}	
	REAL	IMAG	REAL	IMAG	REAL	IMAG	REAL	IMAG
Sphere	4.60	4.59	3.97	3.93	3.81	3.6	4.27	4.32
Dihedral	4.09	4.25	4.26	4.5	3.97	4.38	4.31	4.32
Missile Nose	4.18	4.09	3.77	3.73	3.71	3.67	3.85	3.74
Horizontal wire	4.00	4.22	3.67	3.7	3.70	3.60	3.94	3.89
N_{pq}(f) process	4,01	3,97	3,73	3,69	3,71	3,75	3,98	4,02

Table 2. StDs of the four $S_{pq}(f_0)$ random variables.

We observe that the different illustrated StDs are approximately the same. The NSM statistical model is globally both polarisation channel independent and target independent. Taking into account that the mean of the measured scattering matrix only depends on the studied target, the additive nature of the internal noise sources is consequently demonstrated.

◇ The $N_{pq}(f)$ StDs behaviour versus the frequency

The generalisation of the studied statistical model to the time domain or a radar images domain, demands to characterise the NSM behaviour versus the frequency. Figure 3 presents the four polarisation channel StDs as a function of the frequency. The StDs calculus procedure is performed by measuring 1500 frequential responses of the noise scattering matrix (no target lays down on the AC target support). From each response, the empty AC frequential response, is subtracted. The frequency range is the X band and the gating width, 4 ns.

One can observe the global frequency independence of the four illustrated StDs. The increasing of the StDs when the work frequency gets closer to the boundaries result only from the different signal treatment procedures which are applied to the initial measured frequential signal (Gating).

Moreover, these figures underlines that the StD is polarisation channel independent. It implies that a single StD is sufficient to characterize the whole noise Sinclair matrix.

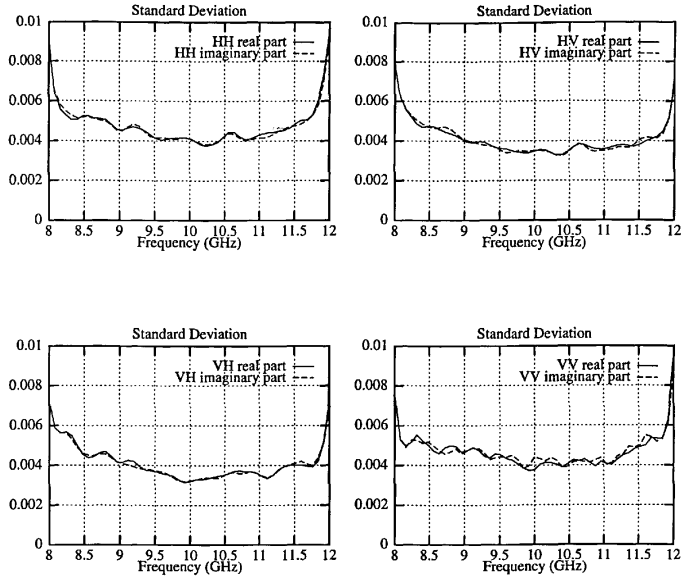

Figure 3. Standard deviation in the X band.

2.1.3 Performance Evaluation of the NSM Statistical Model

The previously internal noise sources model has got two main aspects: it is a statistical model but also a polarimetric model. The performance evaluation of this model has to take into account the two aspects. Therefore, figure 4 represents, at the 10 GHz frequency, the distribution functions (statistical performance evaluation) of the HPs [1] (polarimetric performance evaluation). Only four parameters ($2\,A_0$, $B_0 + B$, C and D) are illustrated owing to the polarimetric nature of the following target. When studying a symmetric [2] target (the sphere previously defined), only the parameters dedicated to the symmetric part target analysis, are different from zero.

To construct the HPs distribution functions, we first have to measure, as previously, a sufficient number of target Sinclair matrices. From this set, we calculate the different HPs sets to finally construct the desired distribution functions. This measured distribution function

[1] Further precisions are given in Section 3.

[2] A symmetric target is a target which has got a symmetric plan containing the radar direction.

is compared with a simulated distribution function whose construction is based on the NSM model. To the mean sphere Sinclair matrix which is deduced from measurement, we add a completely simulated NSM with a 0.004 StD value.

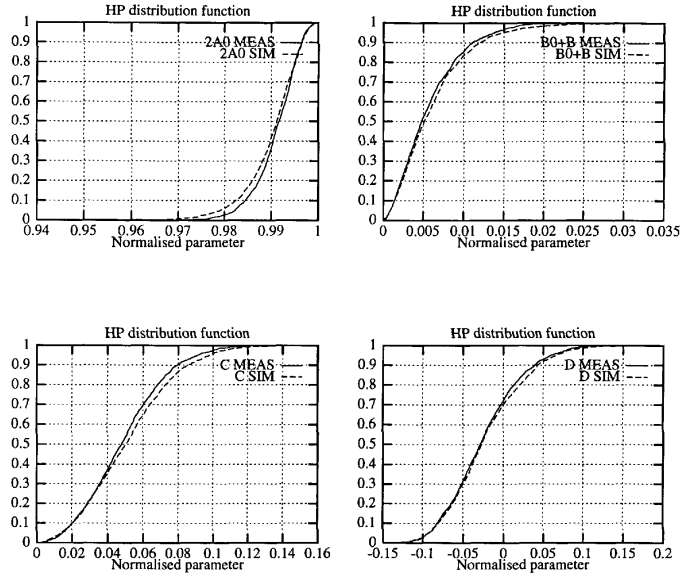

Figure 4. Distribution functions.

Whatever the considered HP is, measured and simulated distribution functions well match. Both the statistical properties and the polarimetric properties of the NSM statistical model are definitely validated.

2.2 In the Spatial Domain

2.2.1 Statistical Model Generalisation to the Time Domain

Considering that the inverse Discrete Fourier Transform is a linear transform, one has the following relation:

$$\mathrm{IDFT}([S(f)]) = \mathrm{IDFT}([S_0(f)]) + \mathrm{IDFT}([N(f)]) \tag{6}$$

Knowing that according to [7], a gaussian process linear transform is a gaussian random process, the temporal NSM $\mathrm{IDFT}([\,N(f)\,])$

defines in the time domain four gaussian random processes $N_{pq}(t)$. The statistical properties of these random processes don't depend on the studied target. Only the StD defining the whole NSM, is consequently modified.

◇ Definitions

- σ_f^{gat} : StD of the real or imaginary part of a $N_{pq}^{\text{gat}}(f)$ gated process
- σ_t : StD of the real or imaginary part of a $N_{pq}(t)$ process
- n_g : number of points which are different from zero in the time domain (application of a gating)

◇ Time standard deviation expression

All calculus steps which are necessary to derive the time StD are given in annexe 1. Finally, the StD in the time domain, expressed as a function of the frequency StD, is:

$$\boxed{\sigma_t = \frac{\sigma_f^{\text{gat}}}{\sqrt{n_g}}} \tag{7}$$

Note that the σ_t StD independence versus the time variable underlines that the added noise has got the same characteristics along the whole longitudinal axis.

◇ Validation of the StD expression

To validate relation 7, Figure 5 represents the time domain StD as a function of the time variable. Each frequential response of the $N_{pq}(f)$ process, from which we deduce the $N_{pq}(t)$ process via an IFFT, is measured by applying a gating. Three different gating, called GATl, GAT2 and GAT3, are applied. Their width are respectively equal to 4 ns, 6 ns and 8.5 ns.

One can observe that outside the temporal window defined by the gating, the time domain StD is near from zero. Within these windows, the time domain StD is constant and keeps the same value whatever the gating is.

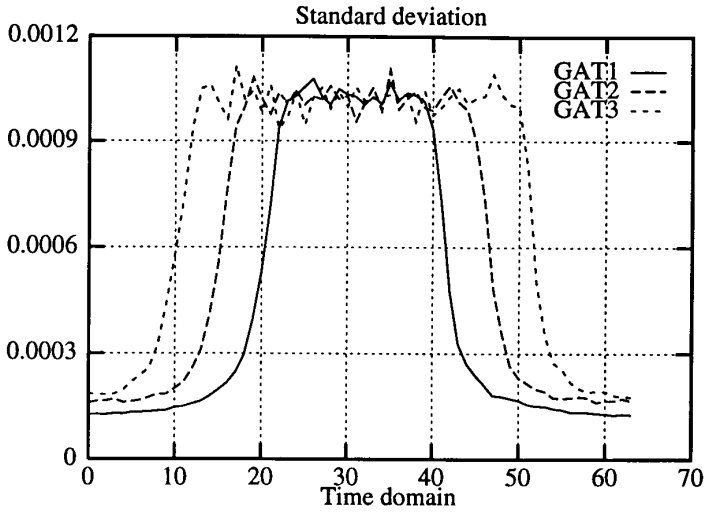

Figure 5. $\sigma_t = g(\text{time})$.

The following table compares the mean $N_{pq}(t)$ process StD, evaluated on the whole window defined by each gating, with the mean $N_{pq}^{\text{gat}}(f)$ process StD, evaluated on the whole X band and weighed by the $1/\sqrt{n_g}$ factor:

	$\overline{\sigma}_{\text{FREQ}}$	$\overline{\sigma}_{\text{TIME}}$	n_g	$\overline{\sigma}_{\text{FREQ}}/\sqrt{n_g}$
GAT1	0.00406	0.00105	17	0.000985
GAT2	0.00499	0.00108	25	0.000998
GAT3	0.00569	0.00109	33	0.000990

Table 3. Time StDs for different gatings.

Whatever the considered gating is, the measured StD values and the relation 11 deduced StD values well match. Relations 11 and 12 are consequently validated.

◇ Conclusion

We have proposed in this part a generalisation of the frequency domain NSM model to the time domain. This model stipulates that the time domain measured scattering matrix is the sum of the target

scattering matrix and of the NSM:

$$[S(t)] = [S_0(t)] + [N(t)] \tag{8}$$

The $[N(t)]$ matrix defines 4 gaussian, ergodic and stationary processes with a zero average and a StD equal to $\sigma_f/\sqrt{n_g}$ ($n_g = n_f$ without any gating).

2.2.2 Statistical Model Generalisation to the Holographic Radar Images Domain

To construct such a model, one has to take into account each radar image calculus step in the evaluation of the desired model statistical characteristics. The following figure sums up the holographic image calculus process that we use.

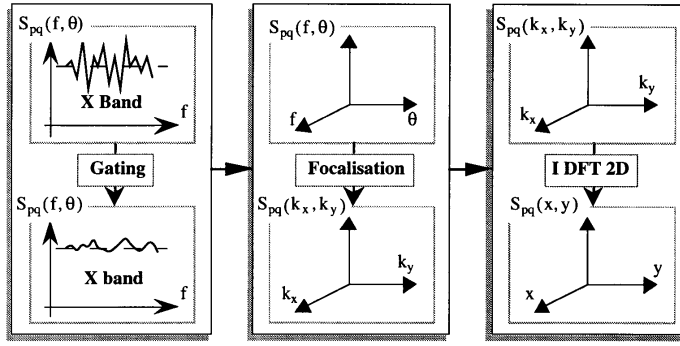

Figure 6. Main steps of the holographic image calculus process.

The construction of an image requires first to measure the desired scattering coefficient on both the azimuth range and the freqeuncy range $(S_{pq}(f,\theta))$. Then, after having applied a gating, one has to calculate the S_{pq} scattering coefficient in the wave vector space $(S_{pq}(k_x,k_y))$. From this expression, we derive the holographic radar image corresponding to the studied scattering coefficient thanks to the Inverse bidimensional Discrete Fourier Transform.

More precisely, the focalisation step [9] is a linear interpolation of the scattering coefficients which are measured in the frequency-azimuth domain. Each wave vector space scattering coefficient $(S_{pq}(k_x,k_y))$ is

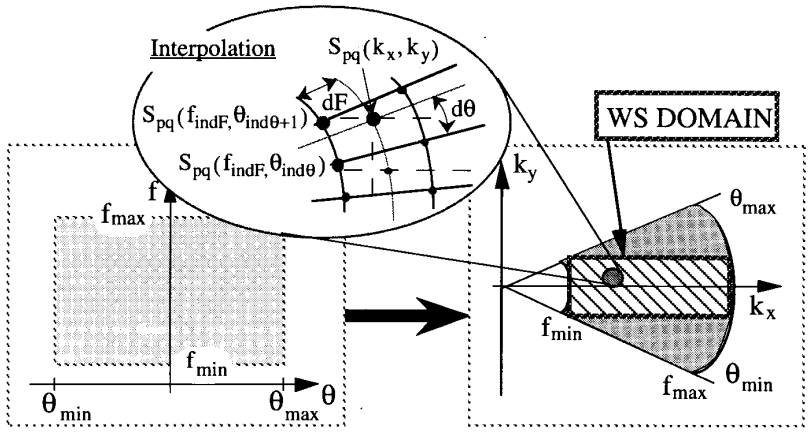

Figure 7. Focalisation step.

the sum of four frequency-azimuth coefficients $(S_{pq}(f, \theta))$:

$$\begin{aligned} S_{pq}(k_x, k_y) = {} & (1 - dF)(1 - d\theta) S_{pq}(f_{indF}, \theta_{ind\theta}) \\ & + dF(1 - d\theta) S_{pq}(f_{indF+1}, \theta_{ind\theta}) \\ & + d\theta(1 - dF) S_{pq}(f_{indF}, \theta_{ind\theta+1}) \\ & + dF d\theta S_{pq}(f_{indF+1}, \theta_{ind\theta+1}) \end{aligned} \tag{9}$$

This procedure allows to express each scattering coefficient in a rectangular area of the wave vector space and consequently to take advantage of the velocity of the bidimensional Fast Fourier Transform.

Each of the radar image calculus steps being a linear transform, one can assess that the NSM model dedicated to the images domain, doesn't depend on the studied target. This NSM defines 4 random processes whose characteristics keep unchanged, except the StD.

The method to derive the expression of the standard deviation of the $N_{pq}(\vec{X})$ process is presented in annexe 2. Finally, we obtain the following expression of the standard deviation:

$$\boxed{\sigma(l_x, l_y) = \sigma_f^{\text{gat}} \sqrt{\frac{n_f}{n_g}} \nu(l_x, l_y)} \tag{10}$$

where

- σ_f^{gat} is the StD of an real or an imaginary part of any gated N_{pq} (f, θ_0) random process.
- $\nu(l_x, l_y)$ is a pixel dependent function (cf. annexe 2)

The $N_{pq}(\vec{X})$ process StD is pixel-dependent owing to the focalisation step.

Figure 8 represents the $\sigma(l_x, l_y)$ expression when applying a gating on each $N_{pq}(f)$ frequency response and the the difference between the simulation StD and the theoretical StD deduced from relation 10 ($\sigma_f^{\text{gat}} = 0.612$ and $n_g = 24$). The simulation consists of calculating an important scattering set in the f - θ space, from which we deduce the corresponding set in the space domain. A StD calculus at each images pixel is finally performed.

The simulation parameters are the following:

- Cardinal set : $N = 1500$
- Frequency range : $[8 \ldots 12]$ GHz
- Points number in the frequency range : $n_f = 64$
- Azimuth range : $[-12 \ldots 12]^\circ$
- Points number in the azimuth range : $n_\theta = 64$

Such a configuration gives to the calculated images, the following dimensions:

- Sample step along the longitudinal axis : 3,69 cm
- Sample step along the transverse axis : 2,29 cm
- Period of the radar image along the longitudinal axis : 2,36 m
- Period of the radar image along the longitudinal axis : 1,85 m

◇ Conclusion

From a NSM statistical model, first validated in the frequency domain then in the time domain, we have defined a NSM statistical model in the radar images domain. This model stipulates that a target Sinclair matrix evaluated in the images domain is the sum of the exact target Sinclair matrix and of a NSM made up of four random processes, with a zero average and a $\sigma(x, y)$ StD:

$$[S(x, y)] = [S_0(x, y)] + [N(x, y)] \tag{11}$$

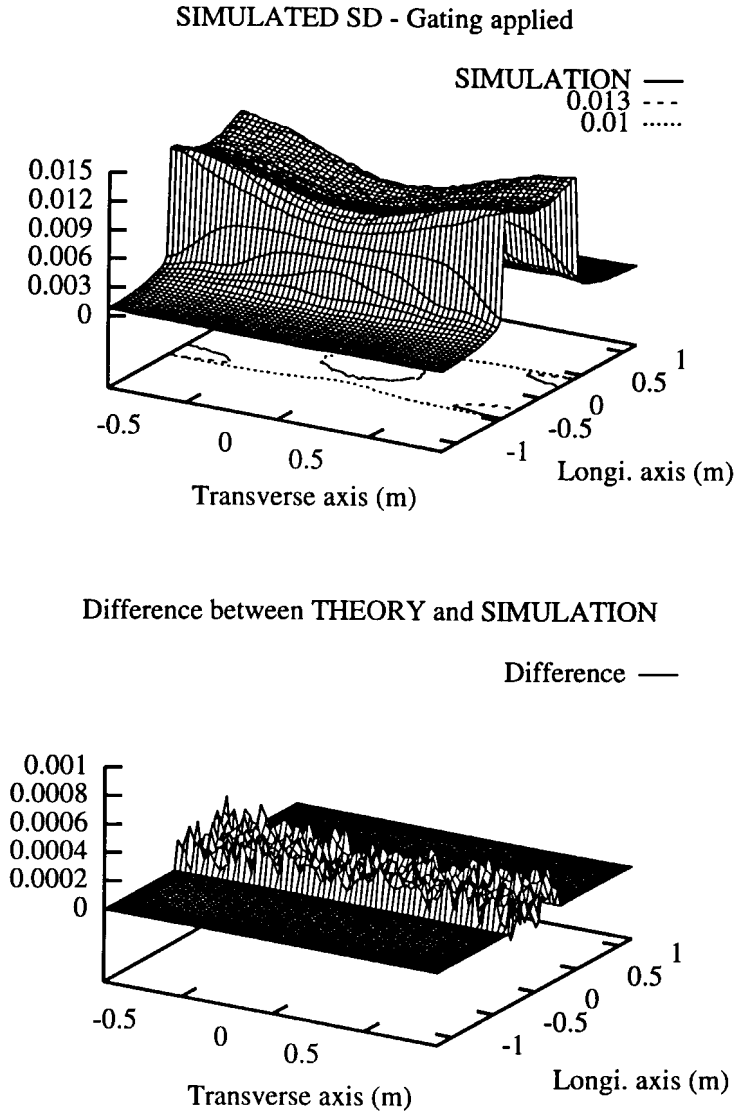

Figure 8. Validation of relation 10.

Thanks to this model, we can now derive, for each pixel, the statistical characteristics of any Huynen parameters. These parameters are calculated by extracting the Sinclair matrix of a scatterer from the pixel which has the maximum value.

3. APPLICATIONS TO THE HPs SENSITIVITY ANALYSIS

None of the applications using HPs as a target classification tool, doesn't estimate its sensitivity versus the noise sources of an AC measurement channel. In this last section, we show the great HPs sensitivity when studying some specific targets and propose an HPs sensitivity prediction model based on the construction of any HP distribution function. A discussion on the use of this model is finally proposed.

3.1 HPs Sensitivity Analysis

Thanks to the build-up of a target independent statistical model of the NSM, one can calculate by simulation any HP statistical characteristic for any target and consequently characterise the sensitivity of this target classification tool versus the noise sources of an AC measurement channel.

We first study a symmetric targets class. This study demonstrates that some HPs become meaningless whatever the backscattered target power is, owing to a too much high sensitivity. A systematic identification of any potentially unstable HP is then conducted, to finally determine the HPs calculus step responsible for this instability.

3.1.1 HPs Sensitivity Characterisation of a Symmetric Targets Class

The chosen HPs sensitivity characterisation tool is the StD. Such a parameter allows one to quantify the HPs dispersal around their mean value.

The symmetric scattering matrices chosen set is defined by the following relation:

$$[S_0] = \begin{bmatrix} S_{hh}^0 & 0 \\ 0 & me^{j\varphi} \end{bmatrix} \tag{12}$$

where m and φ describe respectively the $[0 \ldots |S_{hh}^0|]$ and $[\angle S_{hh}^0 \ldots \angle S_{hh}^0 + 2\pi]$ ranges.

To calculate any HPs StD, one has to first construct a measured scattering matrices set, thanks to one of the models presented in Section 2. From this Sinclair matrices set, we then calculate the corresponding HPs set to finally deduce for each $[S_0]$ Sinclair matrix, the corresponding StD.

The studied HPs are the $2\,A_0$ symmetric generator and the $B_0 + B$ irregularity generator. Each of them is desied but also normalised. [1] Taking into account the σ_N StD value (-48 dBm^2), two values of the hh polarisation channel backscattered power are chosen:

- $\left|S^0_{hh}\right|_{\rm dB} - \left(\sigma^2_N\right)_{\rm dB} = 12.5$ dB
- $\left|S^0_{hh}\right|_{\rm dB} - \left(\sigma^2_N\right)_{\rm dB} = 25$ dB

For these two values, Figure 9 presents the $2\,A_0$ generator sensitivity as a function of the $[S_0]$ Sinclair matrix.

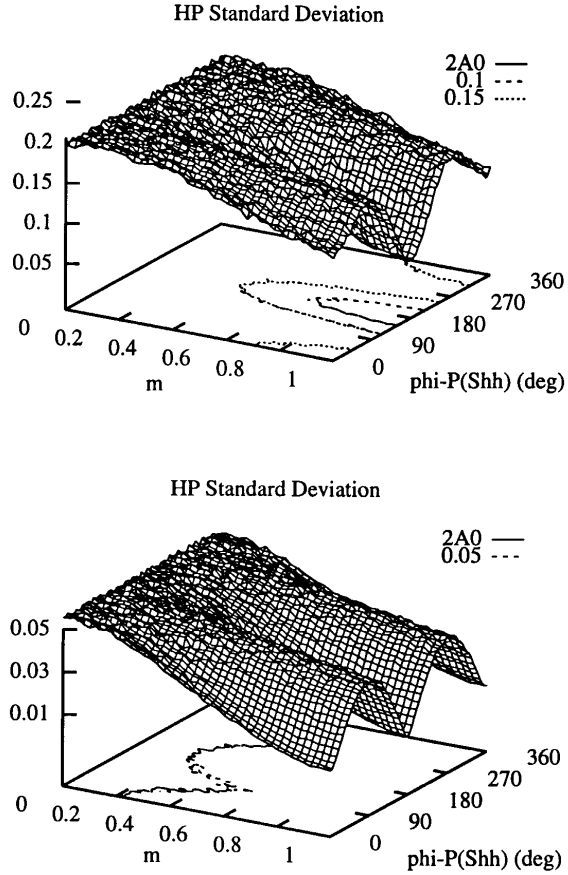

Figure 9. σ_{2A_0} as a function of $[S_0]$.

[1] norm= span($[S]$)=$2(A_0+B_0)$.

This figure first confirms the target dependent sensitivity of each HP owing to the non-linear feature of the HPs calculus procedure. Moreover, one can observe that an increase of the target backscattered power leads to a general decrease of the $2\,A_0$ StD. the $2\,A_0$ generator is all the less sensitive that the target backscattered power increases. Although seeming natural, such a conclusion turns out to be wrong for some others parameters such as the $B_0 + B$ generator.

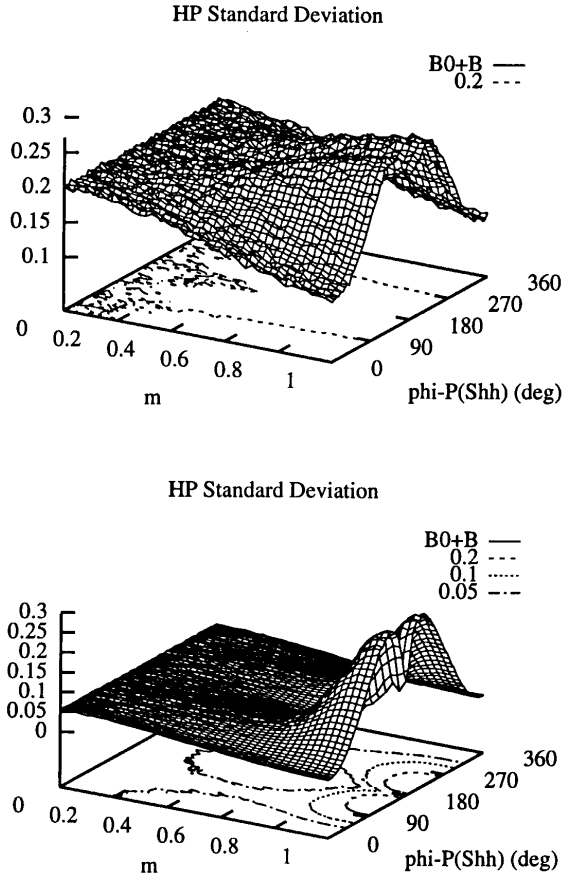

Figure 10. σ_{B_0+B} as a function of $[S_0]$.

On this figure we observe that for some specific $[S_0]$ Sinclair matrices, the $B_0 + B$ StD keeps being high in spite of an increase of the target backscattered power. For these targets, such a parameter has got no more meaning. The following figure illustrates the simulated and measured distribution functions when studying a vertical dihedral at a 8.16 GHz frequency. The distribution functions calculus procedure has been previously described ($\sigma_N = 0004$).

In spite of a high signal to noise ratio (round to 300), the two illustrated curves bears witness of an unstable parameter. The probability to get the $B_0 + B$ generator between 0.65 and 0.85 is inferior to 0.25. This Huynen parameter whose mean value [1] is approximately equal to 0.75, has not to be taken into account in the target classification.

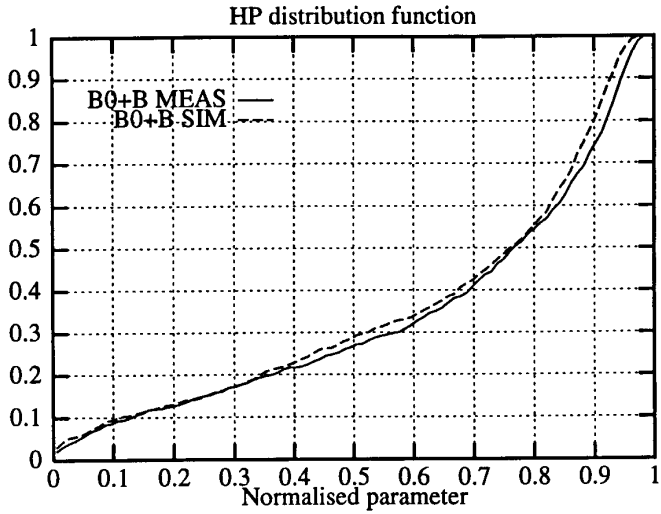

Figure 11. Distribution functions of parameter $B_0 + B$.

3.1.2 Identification of the Potentially Unstable Parameters

In this paragraph, we proceed to a systematic identification of the potentially unstable parameters. We mean by a potentially unstable parameter, a HP which keeps being sensitive in spite of a high target backscattered power. The first point presents the identification

[1] The B_0+B mean value is calculated from the mean scattering matrix which is deduced from the whole scattering matrices set.

procedure which is then applied in the second developed point. Finally, we conclude this paragraph by identifying the HPs calculus step responsible for this instability of some HPs when studying some specific targets.

◇ Method

The identification procedure is of course based on the NSM model, presented in both Sections 1 and 2. Here are the main steps of this procedure.

- step 1: $[S_0]$ Sinclair matrices set
  The adopted method first requires to define a large set of $[S_0]$ Sinclair matrices from which we deduce the different HPs StD. These parameters are desied and normalised according to the previously described normalisation.
  The calculated $[S_0]$ Sinclair matrices are the following:

$$[S_0] = \begin{bmatrix} S_{hh}^0 & m_1 e^{j\varphi_1} \\ m_1 e^{j\varphi_1} & m_0 e^{j\varphi_0} \end{bmatrix} \tag{13}$$

  The S_{hv}^0 and S_{vv}^0 coefficients are respectively defined by the pairs (m_0, φ_0) and (m_1, φ_1):
  - $m_0 \in \left[0 \ldots |S_{hh}^0|\right]$ and $\varphi_0 \in \left[\angle S_{hh}^0 \ldots \angle S_{hh}^0 + \pi\right]$
  - $m_1 \in \left[0 \ldots 2|S_{hh}^0|\right]$ and $\varphi_1 \in \left[\angle S_{hh}^0 \ldots \angle S_{hh}^0 + \pi\right]$

  Although non-exhaustive, this set allows one to consider a wide range among the various Sinclair matrices.
- step 2: maximal StD evaluation
  Once the precedent $[S_0]$ Sinclair matrices set is defined, we calculate the corresponding maximal StD.
- step 3: target backscattered power variation
  We repeat steps 1 and 2 to finally express the maximal StD as a function of the mean target backscattered power that is to say of the S_{hh}^0 coefficient modulus.
  We obtain the following Sinclair matrices sets:

$$[S_0] = \text{SPAN} \begin{bmatrix} S_{hh}^0 & m_1 e^{j\varphi_1} \\ m_1 e^{j\varphi_1} & m_0 e^{j\varphi_0} \end{bmatrix} \tag{14}$$

  where SPAN $\in [1 \ldots 10]$.

◇ Results

Figure 12 illustrates the previously defined maximal StD of any HP, as a function of the SPAN coefficient. One has to note that this simulation is performed with $|S^0_{hh}|_{\mathrm{dB}} - (\sigma^2_N)_{\mathrm{dB}}$ equal to 12.5 dB.

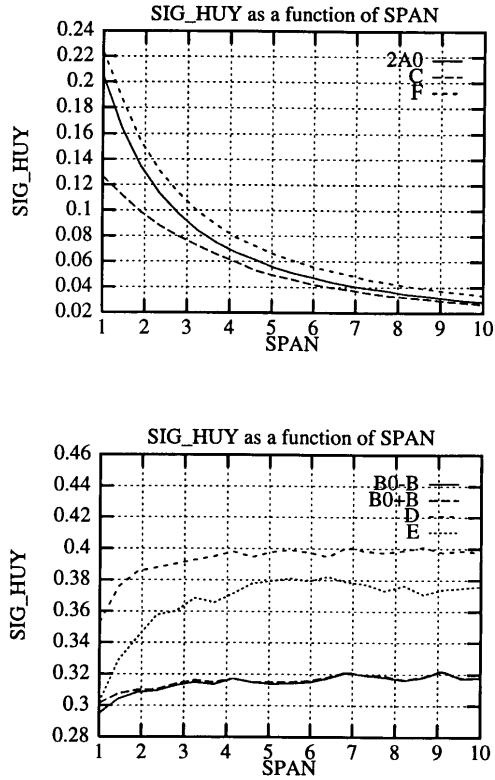

Figure 12. Maximal StD versus the SPAN coefficient.

One can conclude from the analysis of these two figures, on the existence of two kinds of HPs:

- The $2A_0$, C and F parameters whose corresponding maximal StD keeps decreasing as the $[S_0]$ mean backscattered power increases.
- The $B_0 - B$, $B_0 + B$, D and E parameters whose corresponding maximal StD keeps the same level in spite of an increase of the $[S_0]$ mean backscattered power. These parameters are said unstable when, for a specific target, they keep being very sensitive whereas

the target backscattered power is high. This instability is meaningful in so far as the stable parameters of the "same" target are insensitive. For an identical target but backscattering a lower power, one can no more call the Bo+B parameter unstable. It becomes a sensitive parameter as all the others parameters.

◇ Identification of the HPs calculus step responsible for this instability

To have a sense, each HP has to be desied. It implies that whatever the studied target orientation angle facing the line of sight is, the values of the desied HPs keep unchanged. The relations between the desied parameters and the oriented parameters are the following:

$$\varphi = \text{orientation angle} \qquad 2A_0 = 2A_0 \quad B_0 = B_0 \quad F = F$$

$$B = B_\varphi \cos 4\varphi_m + E_\varphi \sin 4\varphi_m \qquad C = \sqrt{C_\varphi^2 + H_\varphi^2}$$

$$D = D_\varphi \cos 2\varphi_m - G_\varphi \sin 2\varphi_m \qquad E = E_\varphi \cos 4\varphi_m - B_\varphi \sin 4\varphi_m$$

$$G = G_\varphi \cos 2\varphi_m + D_\varphi \sin 2\varphi_m \qquad H = 0$$

These relations underline that only the parameters which depend on the orientation angle are potentially unstable. The orientation angle is consequently responsible for the potential instability of the $B_0 - B$, $B_0 + B$, D and E parameters. Indeed, it is impossible to derive with the usual relations and for specific Sinclair matrix, the desired value of φ_m. In another study, we identify these Sinclair matrices and propose a critical analysis of mcaning of some of the Huynen parameters [11].

3.2 Prediction Model of HPs Sensitivity

To ensure the stability of any HP versus the NSM whatever the study domain is, one can construct an HPs sensitivity prediction model, based on the visualisation of the distribution function of the desired HP.

To contruct this distrubtion function, one has first to generate from the single measured Sinclair matrix $[S]$ a sufficient number of Sinclair matrices. This operation is done thanks to the previous statistical models. Then we calculate the HPs corresponding to each generated Sinclair matrix and derive finally from these HPs sets the desired distribution functions. With this model, one is possible to predict the sensitivity of a HPs set, at any pixel of a scattering coefficient radar image.

However, one has to note that the distribution functions are not calculated from an $[S_0]+[N]$ Sinclair matrices set but from the $[S]+[N]$ Sinclair matrices set where $[S]$ is the measured Sinclair matrix. It implies a possible erroneous HP distribution function owing to the non-linear feature of the HPs calculus procedure. To ensure that those calculus procedure doesn't throw back into question our prediction model, two targets are characterised: a symmetric stable target and a near non-symmetric target for which some HPs may become unstable.

◇ A symmetric target study

The studied target has got the following Sinclair matrix:

$$[S_0] = K \begin{bmatrix} 1 & 0.5 \\ 0.5 & 1 \end{bmatrix} \tag{15}$$

We now consider 4 measured Sinclair matrices. Each measured Sinclair matrix $[S_i]$ generated by summing the theoretical Sinclair matrix $[S_0]$ with a sample of the Noise Sinclair matrix $[N]$: $[S_i] = [S_0]+[N_i]$.

From any of these Sinclair matrices, it is quite easy to construct the HPs distribution functions by calculating a $[S_i]+[N]$ Sinclair matrices set. To each HP corresponds five distribution functions: the exact one and those whose construction is based on a single measured Sinclair matrix.

Figure 15 illustrates these distribution functions for two $[S_0]$ backscattered power values versus the variance of the NSM (σ_N^2):

- SPAN $_1$: $\text{span}\,([S_0])_{\text{dB}} - (\sigma_N^2)_{\text{dB}} = 20$ dB [1]
- SPAN $_2$: $\text{span}\,([S_0])_{\text{dB}} - (\sigma_N^2)_{\text{dB}} = 30$ dB

The $2\,A_0$, $B_0 + B$ and D parameters are divided by $\text{span}\,([S_0])$.

We observe that the $2A_0$ distribution functions calculated from a $[S_i] + [N]$ Sinclair matrices set are translated. For the $B_0 + B$ HP, the distribution functions begin to put out of shape compared with the real distribution functions, owing to the range bound proximity. One can not say for all that this prediction model is useless.

Firstly, when the distribution functions are translated, the indicated sensitivity is identical to the real sensitivity illustrated by the $[S_0]$ associated distribution functions. Secondly, the SPAN $_1$ criterion allows one to study targets, in the radar images domain, whose backscattered

[1] $\text{span}\,([S])=|S_{hh}|^2+2|S_{hv}|^2+|S_{vv}|^2$.

power can be no higher than -60 dBm^2.[2] Although slightly put out of shape compared with the real distribution functions, all the $[S_i]$ associated distribution functions, when applying the SPAN$_1$ criterion, bears witness of the $B_0 + B$ parameter sensitivity and consequently lead to the same conclusion.

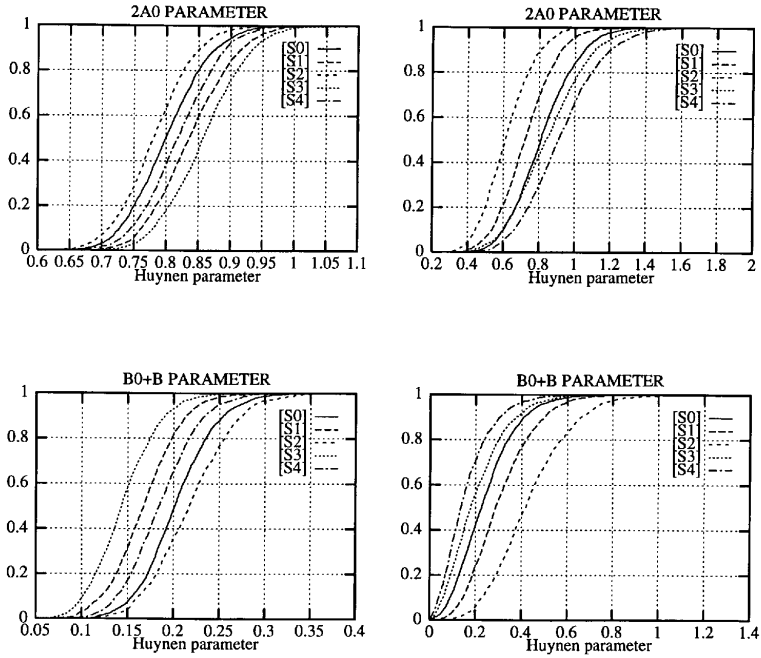

Figure 13. Distribution functions.

◇ A near non-symmetric target study

The studied target has got the following Sinclair matrix:

$$[S_0] = K \begin{bmatrix} 1 & 0.1 \\ 0.1 & e^{j150^\circ} \end{bmatrix} \tag{16}$$

We now consider 4 measured Sinclair matrices. Again, each measured Sinclair matrix $[S_i]$ is generated by summing the theoretical Sinclair matrix $[S_0]$ with a sample of the Noise Sinclair matrix $[N]$.

[2] cf. relation 19: n_f=201, n_g=17, N_{K_x}=194, N_{K_y}=64, σ_f^{gat}=0.004 .

The different distribution functions are calculated for the following criteria:

- SPAN $_1$: span $([S_0])_{\mathrm{dB}} - (\sigma_N^2)_{\mathrm{dB}} = 20$ dB
- SPAN $_2$: span $([S_0])_{\mathrm{dB}} - (\sigma_N^2)_{\mathrm{dB}} = 40$ dB

Only the $B_0 - B$ parameter is studied and is divided by span $([S_0])$. The theoretical value of the $B_0 - B$ generator corresponding to the $[S_0]$ matrix is equal to 0.923.

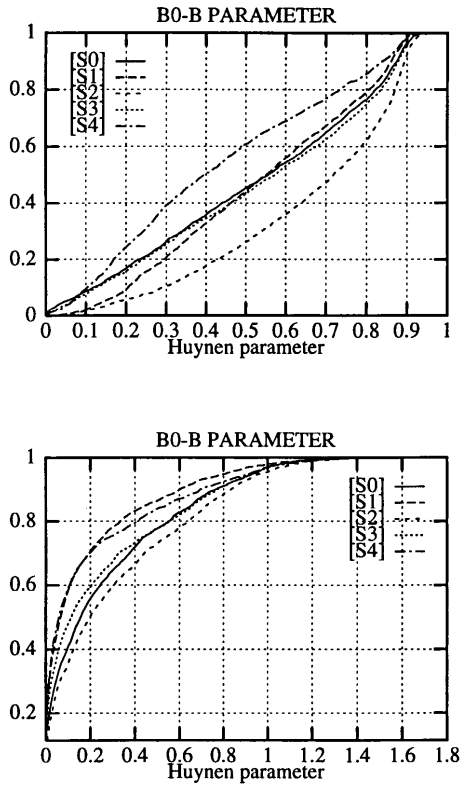

Figure 14. Distribution functions.

All these curves bear witness of the great sensitivity of these parameters. Very sensitive for a 20 dB power difference, the $B_0 + B$ parameter becomes unstable for a 40 dB difference. Our prediction model identifies any HP parameter which is no more held to be reliable.

CONCLUSION

In this paper, we propose a target independent model of the measurement channel noise sources in an AC. This model, first validated in the frequency domain, is then generalised both to the time domain and the holographic radar images domain. For this last model, each holographic image calculus step is taken into account. This concerns the inverse bidimensional FFT but also the frequency response gating and the focalisation step. Thanks to the build-up of such models, we characterise HPs sensitivity and underline the meaningless of some parameters when studying some specific targets. A prediction model of the HPs sensitivity is finally proposed. With such a model, one is possible to quantify for any target the confidence we can accord to an HP and more generally to any polarimetric tool.

ANNEXE 1. TIME STANDARD DEVIATION EXPRESSIONS

In this annexe are presented all the derivations concerning the calculus of the standard deviation σ_t.

◇ Definitions

- σ_f : StD of the real or imaginary part of a $N_{pq}(f)$ non gated process
- σ_f^{gat} : StD of the real or imaginary part of a $N_{pq}^{\text{gat}}(f)$ gated process
- σ_t : StD of the real or imaginary part of a $N_{pq}(t)$ process
- n_f : number of points of a frequency response
- n_g : number of points which are different from zero in the time domain (application of a gating)
- δf : frequential sample step
- δt : time sample step
- Δf : Frequency response band
- Δt : Period of the time response
- $\mathbf{N_{pq}}(\mathbf{n}\delta\mathbf{f})(= N_{pq}(n))$: samples of a $N_{pq}(f)$ non gated frequency response
- $\mathbf{N_{pq}^{gat}}(\mathbf{n}\delta\mathbf{f})(= N_{pq}^{\text{gat}}(n))$: samples of a $N_{pq}(f)$ gated frequency response
- $\hat{\mathbf{N}}_{\mathbf{pg}}(\mathbf{k}\delta\mathbf{t})(= \hat{N}_{pg}(k))$: samples of a $N_{pq}(t)$ time response

◇ Gating dependence of the time domain StD calculus steps

A simple method to derive the time StD expression is to consider the the Inverse Discrete Fourier Transform expression of a frequency signal $N_{pq}(n\delta f)$:

$$\hat{N}_{pg}(k) = \frac{1}{n_f} \sum_{n=-n_f/2}^{n_f/2-1} N_{pq}(n) e^{\frac{2\pi jnk}{n_f}} \tag{17}$$

Assuming that the real or imaginary part of each frequential random variable $N_{pq}(n)$ has a variance equal to σ_f^2 , the real or imaginary part of the $N_{pq}(k)$ random variable has the following expression:

$$\sigma_{pq}^2(k) = \frac{\sum_{n=-n_f/2}^{n_f/2-1} \sigma_f^2}{n_f^2} \tag{18}$$

which gives the following StD:

$$\sigma_{pq}(k) = \frac{\sigma_f}{\sqrt{n_f}} \tag{19}$$

However, this method requires that the $n_f N_{pq}(n)$ gaussian centered random variables are statistically independent that is to say decorrelated. [1] To study the correlation of any ($N_{pq}(n_1)$, $N_{pq}(n_2)$) random variables couple ($n_1 \neq n_2$), one is sufficient to visualise the $N_{pq}(f)$ frequential auto correlation function $R_{hh}(\Delta f)$ (ergodicity and stationarity).

Considering a $N_{hh}(f, \zeta_0)$ random signal at a given event ζ_0 of the sample space, the expression of the corresponding frequential auto correlation coefficient $\rho_{hh}(\Delta f)$ is the following:

$$\begin{aligned} \rho_{hh}(\Delta f) &= \frac{R_{hh}(\Delta f)}{2\sigma_{N_{hh}}^2} \\ &= \frac{1}{2n_f\sigma_{N_{hh}}^2} \sum_{k=0}^{n_f-1} \left(N_{hh}(f_1, \zeta_0) - \mu_{N_{hh}}\right)^* \left(N_{hh}(f_1 + \Delta f, \zeta_0) - \mu_{N_{hh}}\right) \end{aligned} \tag{20}$$

[1] Two gaussian random variables are statistically independent if and only if they are decorrelated [7].

where

- $\mu_{N_{hh}}$ is the residual mean of the $N_{hh}(f)$ process.
- $\sigma_{N_{hh}}$ is the StD of the $N_{hh}(f)$ process (real or imaginary part).

Figure 15 compares the frequential auto correlation coefficient of the $N_{hh}(f)$ gated process with the frequential auto correlation coefficient of the $N_{hh}(f)$ non gated process. Only the real parts are represented.

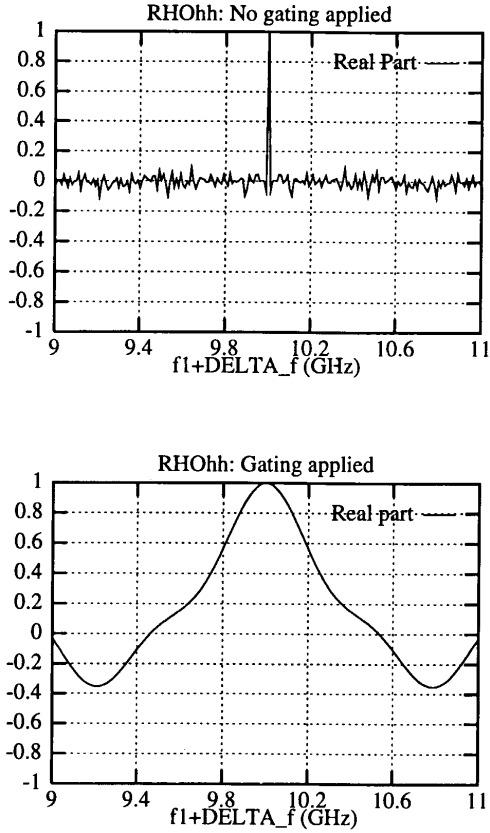

Figure 15. Auto correlation function — Real parts.

For a non-zero value, these two coefficients differ. Without any gating, one can observe the cancelling of the $\rho_{hh}(n\delta f)$ coefficient on the whole frequency range. The $N_{pq}(n_1)$ and $N_{pq}(n_2)$ random variables are then totally decorrelated. On the other hand, when applying a gating, one can no more assess that these two random variables are

decorrelated. Relation 19 is no longer applicable to derive the StD expression.

◇ Time domain StD when applying a gating

Applying a gating induces a width decrease of the useful temporal signal. The frequential sample step is then multiplied by n_f/n_g which implies a decrease of the mean power calculated on the entire X band.

Let's now define P_m and P_m^{gat}, the mean power of respectively the $N_{pq}(f)$ process and the $N_{pq}^{\text{gat}}(f)$ process, calculated on the whole X band:

$$\bullet \quad P_m = \sum_{n=0}^{n_f-1} |N_{pq}(n\delta f)|^2 \tag{21}$$

$$\bullet \quad P_m^{\text{gat}} = \sum_{n=0}^{n_g-1} \left|N_{pq}^{\text{gat}}(n\delta f^{\text{gat}})\right|^2 \tag{22}$$

where band width $= (n_g - 1)\delta f^{\text{gat}} = (n_f - 1)\delta f$.

The relation between these two powers is the following:

$$P_m^{\text{gat}} = \frac{n_g}{n_f} P_m \tag{23}$$

Knowing that for an ergodic process with a zero average, its mean power is equal to its variance [8], one can deduce from relation 23 the following relation:

$$\left(\sigma_f^{\text{gat}}\right)^2 = \frac{n_g}{n_f} P_m \tag{24}$$

By applying the Parseval theorem

$$P_t = \sum_{k=0}^{n_f} |\hat{N}_{pq}(k)|^2 = \frac{1}{n_f} P_m \tag{25}$$

and by assuming the $N_{pq}(t)$ process ergodic, one can express the $N_{pq}(t)$ random process StD as a function of the $N_{pq}(f)$ gated process StD:

$$\boxed{\sigma_t = \frac{\sigma_f^{\text{gat}}}{\sqrt{n_g}}} \tag{26}$$

◇ Note

By assuming that the $N_{pq}^{\text{gat}}(f)$ process defines n_f statistically independent random variables with a σ_f^{gat} StD weighed by a $\sqrt{n_f/n_g}$ factor, the first method would give the same results:

$$\sigma_t = \frac{1}{\sqrt{n_f}} \left(\sqrt{\frac{n_f}{n_g}} \sigma_f^{\text{gat}} \right) = \frac{\sigma_f^{\text{gat}}}{\sqrt{n_g}} \tag{27}$$

ANNEXE 2. STANDARD DEVIATION EXPRESSION IN THE HOLOGRAPHIC DOMAIN

This annexe presents the different steps to derive the expression of the standard deviation in the holographic domain first when no gating is applied then when a gating is applied.

◇ Radar images domain StD calculus - NO gating

In so far as no gating is applied, any $N_{pq}(f_0, \theta_0)$ random variable is statistically independent of any $N_{pq}(f_1, \theta_0)$ random variable, provided that f_0 differs from f_1. Concerning the two $N_{pq}(f, \theta_0)$ and $N_{pq}(f, \theta_1)$ random processes ($\theta_0 \neq \theta_1$), even in the presence of a gating, they are statistically independent and with identical characteristics. The calculus of the images domain StD is consequently based on the bidimensional IDFT procedure.

Let's now consider the $N_{pq}(l_x \delta_x, l_y \delta y)$ coefficient expression in the radar images domain:

$$N_{pq}(l_x \delta x, l_y \delta y) = \frac{1}{N_{k_x} N_{k_y}} \sum_{n_y=-N_{k_y}/2}^{N_{k_y}/2} \sum_{n_x=-N_{k_x}/2}^{N_{k_x}/2} N_{pq}[n_x \delta k_x, n_y \delta k_y] e^{j(n_x \delta k_x l_x \delta x + n_y \delta k_y l_y \delta y)} \tag{28}$$

where

- δx and δy are the sample steps of an holographic radar image.
- δk_x and δk_y are the sample steps along respectively the longitudinal axis and the transverse axis in the wave vector space.
- N_{k_x} and N_{k_y} are the points numbers along respectively the longitudinal axis and the transverse axis in the wave vector space.

By changing the $N_{pq}(n_x\delta k_x, n_y\delta k_y)$ coefficients by its $N_{pq}(n_f\delta f, n_\theta\delta\theta)$ coefficients depending expression, we obtain:

$$N_{pq}(l_x\delta x, l_y\delta y) = \frac{1}{N_{k_x}N_{k_y}} \sum_{n_y=-N_{k_y}/2}^{N_{k_y}/2} \sum_{n_x=-N_{k_x}/2}^{N_{k_x}/2} \sum_{i_{foc}=0}^{n_{foc}-1} \beta(n'_f, n'_\theta) N_{pq}[n'_f\delta f, n'_\theta\delta\theta] e^{j(n_x\delta k_x l_x\delta x + n_y\delta k_y l_y\delta y)} \tag{29}$$

where

- $n'_f = n_f(n_x, n_y, i_{foc})$
- $n'_\theta = n_\theta(n_x, n_y, i_{foc})$
- n_{foc} is the coefficients number of the f - θ space, which are utilised for the calculus of a single wave vector space coefficient $N_{pq}[n_x\delta k_x, n_y\delta k_y]$.
- $\beta(n'_f, n'_\theta)$ is a real coefficient whose expression depends on the kind of the focalisation which is applied.

Knowing that the $N_{pq}(n_f, n_\theta)$ random variables are two by two statistically independent, one can deduce from relation 29 of the StD of the $N_{pq}(l_x, l_y)$ random variables:

$$\boxed{\sigma(l_x, l_y) = \sigma_f \nu(l_x, l_y)} \tag{30}$$

where

- σ_f is the StD of an real or an imaginary part of any $N_{pq}(f, \theta_0)$ random process.
- $\nu(l_x, l_y) = \frac{1}{N_{k_x}N_{k_y}} \sqrt{\sum_{n_f, n_\theta \in [\text{WS DOMAIN}]} |\gamma(n_f, n_\theta, l_x, l_y)|^2}$ [1]

  with

  $$\gamma(\mathbf{n_f}, \mathbf{n_\theta}, l_x, l_y) = \sum_{\substack{(n_x, n_y, i_{foc}) \text{ such that} \\ n'_f = \mathbf{n_f} \text{ and } n'_\theta = \mathbf{n_\theta}}} \beta(n'_f, n'_\theta) e^{j(n_x\delta k_x l_x\delta x + n_y\delta k_y l_y\delta y)}$$

◇ Radar images domain StD calculus – WITH gating

Because of the gating, relation 30 is no more applicable owing to the $N_{pq}(f_0, \theta_0)$ variables statistical dependence.

[1] Cf. Figure 7 for the WS DOMAIN meaning.

However, when having calculated the gated StD in the time domain, we underlined that the gatingless method was applicable, provided that the $N_{pq}(f_0)$ variables were assumed statistically independent and that their StD was weighed by an $\sqrt{n_f/n_g}$ factor.

By applying this method, one can deduce from relation 30 the StD expression of the image domain NSM when applying a gating:

$$\boxed{\sigma(l_x, l_y) = \underbrace{\sigma_f^{\text{gat}} \sqrt{\frac{n_f}{n_g}}}_{\sigma_f} \nu(l_x, l_y)} \tag{31}$$

where more precisely $\sigma(l_x, l_y)$ is the StD of the real or the imaginary part of any $N_{pq}(\vec{X})$ process.

ACKNOWLEDGEMENTS

The authors wish to thank the CEA-CESTA (Le Barp FRANCE) for suggesting and supporting this study.

REFERENCES

1. Cloud, S. R., E. Pottier, "Review of target decomposition theorem in radar polarimetry," *IEEE Transaction on Geoscience and Remote Sensing*, Vol. 34, No 2, March l996.
2. Titin-Schnaider, C., "A polarimetric tool for radar targets analysis," *Proceedings of the third international workshop on radar polarimetry*, 1995.
3. Huynen, J. R., "The Stokes matrix parameters and their interpretation in terms of physical target properties," *Proceedings of the first international workshop on radar polarimetry*, 1990.
4. Huynen, J. R., "Phenomenological theory of radar targets," *Ph.D. Thesis*, P.Q.R. Press, First Revision, 1987.
5. Boerner, W.-M., S. K. Chaudhuri, B.-Y. Foo, "A validation analysis of the Huynen's target-descriptor interpretations of the Mueller matrix elements in polarimetric radar returns using Kennaugh's physical optics impulse response formuation," *IEEE T.A.P.*, Vol. 34, No 1, 87–93, Jan. l986.
6. Riegger, S., W. Wiesbeck, "A complete error Model for free space polarimetric measurements," *IEEE T.A.P.*, Vol. 39, No 8, Aug. l991.

7. Blanc-Lapierre, A., B. Picinbono, "Fonctions aléatoires," *Collection technique et scientifique des Télécommunications*, Éditions Masson.
8. Urkowvitz, H., *Signal Theory and Random Processes*, Artech House, 1983.
9. Morvan, S., J. Garat, "Signal processing methods for RCS measurements," *Revue scientifique et technique de la DAM*, No 8, Sep. 1993.
10. Huynen, J. R., "Physical relevance in radar target polarimetry," *Proceedings of the Second International Workshop on Radar Polarimetry*, 1992.
11. Priou, L., Y. Le Helloco, G. Chassay, "A study of the desying process of a radar target, applied to a critical analysis of the mcaning and sensibility of some Huynen parameters," *Microwave and Optical Tech. Lett.*, Feb. 1997.